BASIC SCIENCE

Nanomedicine: Nanotechnology, Biology, and Medicine
10 (2014) 1549–1558

Original Article

nanomedjournal.com

The orientation of the neuronal growth process can be directed via magnetic nanoparticles under an applied magnetic field

Cristina Riggio, PhD[a], M. Pilar Calatayud, PhD[b,d], Martina Giannaccini, PhD[a,c], Beatriz Sanz, MsC[b], Teobaldo E. Torres, MsC[b,d,e], Rodrigo Fernández-Pacheco, PhD[b,e], Andrea Ripoli, PhD[f], Manuel Ricardo Ibarra, MsC[b,d], Luciana Dente, MsC[c], Alfred Cuschieri, MD[a], Gerardo F. Goya, PhD[b,d], Vittoria Raffa, PhD[a,c,*]

[a]*Institute of Life Science, Scuola Superiore Sant'Anna, Pisa, Italy*
[b]*Instituto de Nanociencia de Aragón, Universidad de Zaragoza, Mariano Esquillor, Zaragoza, Spain*
[c]*Department of Biology, Università di Pisa, Pisa, Italy*
[d]*Departamento de Física de la Materia Condensada, Pedro Cerbuna, Zaragoza, Spain*
[e]*Laboratorio de Microscopias Avanzadas (LMA), Universidad de Zaragoza, Mariano Esquillor, Zaragoza, Spain*
[f]*Fondazione Toscana "Gabriele Monasterio", Via Giuseppe Moruzzi, Pisa, Italy*

Received 24 October 2013; accepted 23 December 2013

Abstract

There is a growing body of evidence indicating the importance of physical stimuli for neuronal growth and development. Specifically, results from published experimental studies indicate that forces, when carefully controlled, can modulate neuronal regeneration. Here, we validate a non-invasive approach for physical guidance of nerve regeneration based on the synergic use of magnetic nanoparticles (MNPs) and magnetic fields (Ms). The concept is that the application of a tensile force to a neuronal cell can stimulate neurite initiation or axon elongation in the desired direction, the MNPs being used to generate this tensile force under the effect of a static external magnetic field providing the required directional orientation. In a neuron-like cell line, we have confirmed that MNPs direct the neurite outgrowth preferentially along the direction imposed by an external magnetic field, by inducing a net angle displacement (about 30°) of neurite direction.

From the Clinical Editor: This study validates that non-invasive approaches for physical guidance of nerve regeneration based on the synergic use of magnetic nanoparticles and magnetic fields are possible. The hypothesis was confirmed by observing preferential neurite outgrowth in a cell culture system along the direction imposed by an external magnetic field.

Key words: Nerve regeneration; Magnetic nanoparticle; Magnetic field; Neurite outgrowth orientation; Physical guidance

Nerve regeneration and recovery of nerve function have been a major issue in neuroscience in regards to the treatment of injured neurons after accidents or degenerative diseases.[1] The regeneration of peripheral nerves exemplifies the plasticity which exists within the nervous system. Following an injury to a peripheral nerve, the section distal to the injury site degenerates. Functional recovery is then totally dependent on the growth and extension of axons from the proximal end across the injured site until they reach their distal target, e.g., denervated muscle.[2] In humans, axonal regeneration occurs at a rate of about 2-5 mm/day; and thus significant complete injuries (neurotmesis) can take many months for effective return of function.[3] Extensive research in

Abbreviation: MNPs, Magnetic nanoparticles; M, Magnetic fields; NFs, Neurotrophic factors; NGF-β, Nerve growth factor beta; BSA, Bovine serum albumin; NGF_{fluor}, Fluoscently labelled NGF-β; TPF, Tetrafluorophenyl; f-MNP, MNP labelled with NGF_{fluor}; FBS, Fetal bovine serum; PLL, Poly-L-lysine; TEM, Transmission electron microscopy; HAADF, High angle annular dark field; EDS, Energy-dispersive X-Ray Spectroscopy; EDAX, EDS detector; SEM, Scanning electron microscopy; PI, Propidium iodide; T_d, Doubling time; PEI, Polyethylenimine; SPION, Superparamagnetic iron oxide nanoparticles; p-TrkA, Phosphorylated TrkA; K, Control; P, Pellet; S, Supernatant; FIB, Focused ion beam; STEM, Scanning TEM; FEM, Finite element modelling.

The authors declare no conflict of interest.

*Corresponding author.
E-mail addresses: c.riggio@sssup.it (C. Riggio), pilarcs@unizar.es (M.P. Calatayud), m.giannaccini@sssup.it (M. Giannaccini), beasanz@unizar.es (B. Sanz), teo@unizar.es (T.E. Torres), pacheco@unizar.es (R. Fernández-Pacheco), andrearipoli@ftgm.it (A. Ripoli), ibarra@unizar.es (M.R. Ibarra), ldente@biologia.unipi.it (L. Dente), a.cuschieri@sssup.it (A. Cuschieri), goya@unizar.es (G.F. Goya), vraffa@biologia.unipi.it (V. Raffa).

http://dx.doi.org/10.1016/j.nano.2013.12.008
1549-9634/

bioengineering has been focused on the development of innovative strategies for reducing this prolonged recovery time. The underlying concepts of these strategies involve physical and biochemical guidance i) to direct axonal re-growth and ii) to stimulate axonal elongation across the nerve lesion site. For a long time, neuroscientists have focused on biochemical guidance cues such as molecules capable of orientating migrating and growing cells (e.g., netrins, ephrins, semaphorins) and factors influencing neuronal growth (e.g., growth factors, neurotransmitters, glial cells and extracellular matrix proteins).[4] However, exclusive focus on biochemical processes involved in neuronal regeneration has not so far resulted in significant therapeutic gains. An alternative approach is the "guidance therapy" based on the use of scaffolds (autologous tissue grafts, non-autologous tissue grafts, natural based materials, synthetic materials, etc.) working as "nerve guides" or "nerve guidance channels". They provide a conduit during the nerve regeneration process for the diffusion of growth factors secreted by the injured nerve ends and to limit the injury site infiltration by scar tissue.[5-8]

The importance of mechanical factors for the nervous system has been appreciated only recently. It has become widely accepted that cellular tension is a crucial factor in neuronal development.[9] The idea that tension is involved in the morphogenesis of the nervous system arose in the late 1970s, when experimental pioneering work revealed that neuronal processes in vitro are under tension.[10] Later, it was demonstrated that the external application of mechanical tension alone is sufficient to initiate axonal outgrowth.[11] Neurite initiation and elongation as functions of the applied tensile force were generally studied using glass microneedles but, recently, Fass et al reported the use of magnetic beads for force application.[12]

Although the role of mechanical force for neurite initiation and elongation is a well investigated topic, its influence in directing axonal re-growth is poorly studied. The control of directional movement is obviously a crucial issue in nerve regeneration as regeneration cannot occur until the proximal end of the injured nerve reaches its destination. During the regeneration process, neurons send out the leading tips of their processes called growth cones. They are highly motile structures that provide the machinery to move forward. Recent work suggests that growth cones also generate forces (through cytoskeletal dynamics, kinesin, dynein, and myosin) which induce axonal elongation, and axons lengthen by stretching.[13] They also possess detectors of guidance cues that translate environmental cues into directional movement and thus guide neuronal processes toward their destination.[14] Guidance cues are classically understood to be attractive or repulsive molecules, capable of orientating neuronal cells. Generally, a growth cone's response to a certain guidance cue depends on several factors and it is difficult to gain control on this process. An alternative approach proposed in literature is to introduce topographic cues to guide neuronal navigation.[15-18] Although several reports have demonstrated the cell culture benefit of these cues, they usually fail when tested therapeutically. One problem is that the non-invasive delivery of these cues is difficult if not impossible to achieve. Here, we validate an alternative approach for physical guidance. Specifically, we demonstrate that magnetic nanoparticles (MNPs) and magnetic fields (Ms) can be used for physical guidance of neuronal processes. We found that the application of a tensile force to a neuron or an axon can stimulate neurite initiation or axon elongation in the desired direction. In this work, MNPs are used to generate these tensile forces under the effect of an external magnetic field and to achieve directional orientation (Figure 1).

The first draft of this idea was reported by a patent submitted in 1998 (US6132360 A) which describes a methodology based on MNPs which are actively incorporated into neurons (and their axons) of a severed or interrupted nerve. This is then exposed to an external magnetic field which is moved longitudinally to the severed/interrupted nerve, thereby stretching the MNPs-loaded neurons and their axons along the desired axis for bringing the gap. To our knowledge, no practical demonstration of this concept has been provided to date and our work represents the first proof of concept.

This methodology has the potential for clinical translation as static magnetic fields are extensively used in medical imaging.[19] Additionally, magnetic nanoparticles are employed in biomedicine. Currently, many clinical diagnostic/therapeutic tools use MNPs, e.g., MRI contrast agents in magnetic resonance imaging and magnetic hyperthermia, vectors for drug delivery and magnetic cell separation, etc.[20-22]

Additionally, in combination with recent advances in functionalization chemistry MNPs can be easily functionalised with biological molecules, e.g., neural binders to enhance MNP binding to neuronal cells[23,24] or neurotrophic factors (NFs) to stimulate peripheral neurons to regenerate their axon[25] or specific antibody to track signaling endosome and control their subcellular localization in order to alter growth cone motility and to halt neurite growth.[26]

In the present work, we produced and characterised MNPs functionalised with nerve growth factor beta (NGF-β), demonstrating that these particles are able to trigger PC12 differentiation in a neuronal phenotype and, most importantly, to direct the orientation of newly formed neurites.

Methods

Functionalisation of MNPs

MNPs were synthesised by a modification of the well-established oxidative hydrolysis method (i.e., the precipitation of an iron salt in basic media with a mild oxidant).[27] Specifically, in situ polymer coating was achieved by adding polyethylenimine (PEI, 25 kDa) during the reaction, as described in a previous work.[28]

The protein (a mixture NGF-β /BSA 1:6 w/w) (Sigma, N1408) was labelled with Alexa Fluor 488 (Life Science, A10235). TFP ester of the dye efficiently reacted with primary amines of proteins. Purification through a size exclusion resin allowed to discard the unincorporated dye. The concentration of the purified labelled protein was evaluated by UV–vis analysis. The absorbance spectrum revealed the presence of two peaks: at 280 and 494 nm, typical of proteins and Alexa Fluor 488, respectively (Figures S1-2, supplementary material).

The functionalization of the particles was carried out by adding the labelled protein (concentration of NGF_{fluor} 35 $\mu g ml^{-1}$) to MNPs (500 $\mu g ml^{-1}$). The resulting suspension was dispersed at

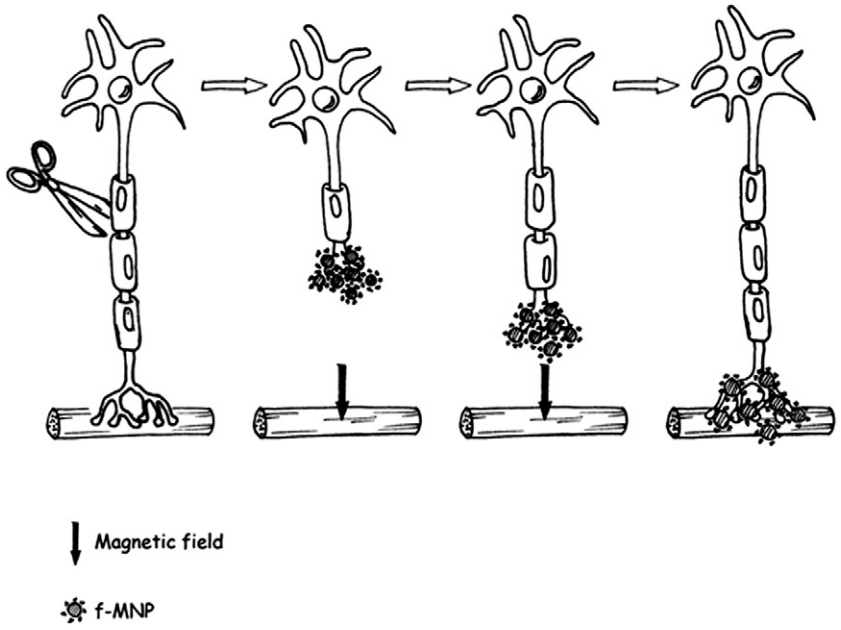

Figure 1. Nerve regeneration mediated by MNPs. MNPs bind to the injured nerve, a magnetic field is thus applied. MNPs create a mechanical tension which stimulates nerve regeneration in the direction imposed by the magnetic force. This physical guidance directs more efficiently the regeneration of the injured nerve from the proximal toward the distal stump.

room temperature for three hours with stirring. Unbound NGF_{fluor} was removed and f-MNPs were re-suspended in water.

The amount of NGF_{fluor} bound to the surface of MNPs was calculated by subtraction, i.e., by measuring the absorbance at 280 nm of the supernatant derived from the previous washing steps. The NGF_{fluor} concentration was obtained by using a calibration curve obtained with a known amount of NGF_{fluor} protein. The amount of NGF_{fluor} adsorbed on MNP surface was about 10(±5) μg of NGF_{fluor} per mg of MNPs (n = 6).

f-MNPs were characterized by Z-potential (Zeta sizer Nano™ from Malvern Instrument) and by Western blot analysis on protein extracts from PC12 cells using phospho-TrkA (Tyr490) Antibody (Cell Signaling, 9141).

Cell culture

Rat pheochromocytoma PC12 cells obtained from American Type Culture Collection (ATCC) were cultured in Dulbecco's modified Eagle's medium with 10% horse serum, 5% fetal bovine serum (FBS), 100 IU/ml penicillin, 100 μgml^{-1} streptomycin and 2 mM L-glutamine. Cells were cultured in poly-L-lysine (PLL, Sigma, P1274) coated dishes and maintained at 37 °C in a saturated humidity atmosphere of 95% air and 5% CO_2. For cell differentiation, PC12 cells were incubated in serum-reduced medium (2% FBS).

TEM and SEM/FIB analysis

Transmission electron microscopy (TEM) was performed using a FEI Tecnai T20 microscope, operating at acceleration voltage of 200 kV. STEM-HAADF images were obtained in a FEI Tecnai F30 microscope operated at an acceleration voltage of 300 kV. The microscope was equipped with a high angle annular dark field (HAADF) detector and an Energy-dispersive X-Ray Spectroscopy (EDS) detector (EDAX). The preparation of the cells was made by seeding PC12 cells on 6 well plate previously treated with PLL (10 μgml^{-1}) at a density of $3 \cdot 10^5$ cells/well. Subsequently, the growth medium was removed and replaced with the reduced medium containing f-MNPs (10 μgml^{-1}). After 24 h of incubation cells were prepared for TEM imaging according to a standard protocol (supplementary material).

SEM/FIB cross sectioned cells were analyzed using scanning electron microscopy (SEM INSPECT F50, FEI Company) and dual-beam FIB/SEM (Nova 200 NanoLab, FEI Company). PC12 cells were grown on coverslip coated with PLL and treated with f-MNPs (10 μgml^{-1}). After 24 h of incubation the cells were washed with PBS, fixed and dehydrated (additional information in supplementary material). After drying the samples were sputtered with 30 nm of gold. SEM images were taken at 5 and 30 kV with a FEG column, and a combined Ga-based 30 kV (10 pA) ion beam was used to cross-section single cells. These investigations were completed by EDS for chemical analysis.

Cell viability

For dose–response studies, PC12 cells were incubated for 72 h in reduced culture medium modified with f-MNPs (1-100 μgml^{-1}).

Cell cytotoxicity was assessed using a FACScan cytometer (Becton Dickinson). Acquired data were analysed using CellQuest Pro software (version 3.4). Before acquisition, adherent cells were washed with PBS, detached by trypsinization and suspended in measuring buffer containing propidium iodide (PI) 0.5 μgml^{-1}. Controls (normal cells, cell treated with PI and cells incubated with f-MNPs) were first used as references for

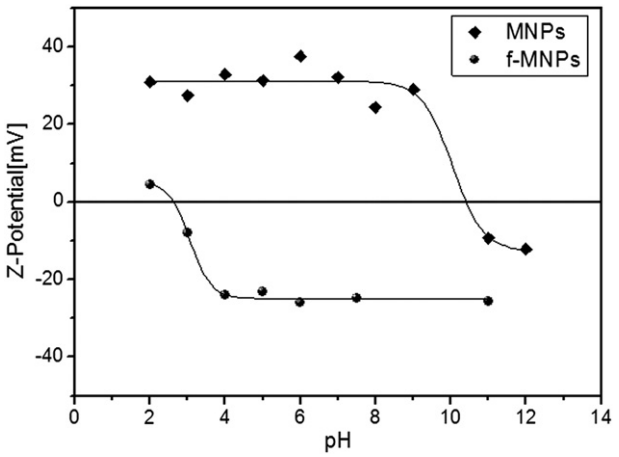

Figure 2. Zeta potential vs pH for f-MNPs (grey circles) and MNPs (black rhombi). The positive value of the MNPs is due to the presence of the free PEI amino groups on the particle surface, while the negative value of f-MNPs is in agreement with the isoelectric point of the proteins.

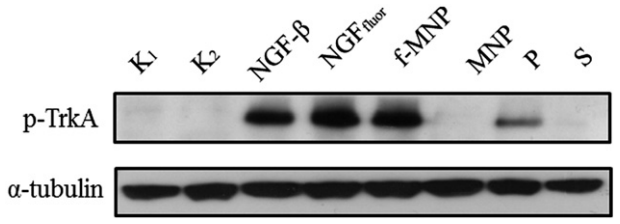

Figure 3. Western blot analysis (p-TrkA 140 kDa and α-tubulin 50 kDa) carried out on PC12 cell extracts. The cells were grown in serum supplemented medium (K_1) or starved in serum-reduced medium (all other lanes): untreated control (K_2), treatment with NGF-β, NGF_{fluor}, f-MNP, MNP, pellet (P) and supernatant (S). P and S were obtained from magnetic separation of a mixture f-MNPs:medium (1:10). The bioactivities of NGF-β, NGF_{fluor} and f-MNP are similar; the presence of p-TrkA was found in the pellet but not in the supernatant which reveals the stability of f-MNPs in the medium. For all treated samples the concentration of particles and NGF was 10 μgml^{-1} and 80 $ngml^{-1}$, respectively.

Table 1
Effect of f-MNPs on PC12 cell line.

	10 μgml^{-1}	20 μgml^{-1}	50 μgml^{-1}	100 μgml^{-1}
Cytoxicity (%)	1.4 ± 0.4	1.3 ± 0.5	2.2 ± 0.4	3.8 ± 0.8
Cell doubling time (h)	46.9 ± 6.5	45.7 ± 11.4	48.6 ± 13.8	61.4 ± 15.1

Cell viability assay was carried out by PI staining via flow cytometry (mean ± s.e.m., n=6, p<0,0001). Cell doubling time was calculated as described in Methods (mean ± s.e.m., n=6, p=0.13). One-way ANOVA.

adjusting the voltage controlling forward scatter and side scatter. 10^6 events/sample were acquired. Results were expressed as a percentage of red-stained cells over the total cell number. For the evaluation of the cell doubling time, cells were removed by trypsinization and counted in a Burker's chamber. Doubling time (T_d) was calculated, assuming a constant growth rate, by using the following formula: $T_d = (t_1 - t_0) \cdot \ln(2)/\ln(q_1/q_0)$, where q_0 represents the cell number at time t_0 and q_1 the cell number at time t_1.

Magnetic field

Numerical simulations using Finite Element Modelling (FEM) were used to design the magnetic applicator. The magnetic field was generated by a magnetic applicator composed of eight magnets arranged in a Halbach-like cylinder configuration (Figure S6.B, supplementary material). The central space was designed to fit the current sample holders, i.e., 3-cm Ibidi Petri dishes. This configuration guarantees in the central space a constant magnetic force with a radial direction outwards.

Neurite orientation

PC12 cells were seeded in Ibidi Petri dishes (Ibidi, 80156) pre-coated with PLL 1 μgml^{-1}. After 24 h from seeding, cells were treated with 10 μgml^{-1} of f-MNPs mixed to reduced serum medium. Cells were incubated again for 24 h to allow the nanoparticles to interact with cells and to induce differentiation. The Petri dish was put inside the magnetic applicator. After 3 days, the angle θ between the direction of each neurite and the radial direction outwards, the neurite length and the neurite number were measured. Neurite orientation was quantified as orientation index which was defined as $Oi = cos(\theta)$, with $0 < \theta < \pi$ ($Oi \sim 1$ when the neurite has the radial direction outwards). Neurites were selected by fixing a cut-off of 10 μm in length. Experiments were carried out in 6-plicate. For each experiment, 25 pictures were acquired. For each picture an average of 460 neurites was counted. Analysis was performed by using image analysis software "Image J" (http://rsb.info.nih.gov/ij/).

Statistics

The distributions of the variables were found to be no normal by Kolmogorov–Smirnov test; therefore, their values were expressed as median and interquartile range. After normalization with rank transform,[29] the effect of treatments was assessed by one-way analysis of variance. Specifically, Kolmogorov–Smirnov test furnished a statistic $D = 0.1047$ ($P < 0.001$), $D = 0.119$ ($P < 0.001$) and $D = 0.2229$ ($P < 0.001$) for neurite orientation, length and number, respectively; after rank transform, the corresponding Kolmogorov–Smirnov statistics were $D = 0.0018$ ($P = 1$), $D = 0.0006$ ($P = 1$) and $D = 0.0874$ ($P = 0.358$). Treatments were compared to the single control group with a post-hoc Dunnett's test. Multiple comparisons between groups were performed with Bonferroni correction. A P value less than 0.05 was considered to be statistically significant. Statistical analyses were performed with R statistical software.

Results

The home-made MNPs used in this work exhibit a core size of 25 nm and a value of saturation magnetization of 58 Am^2kg. A large magnetization value is a crucial parameter for maximizing the force exerted by the external magnetic field on the MNP-axon complex. The presence of a thin polymer coating (about 0.7-0.9 nm) was observed from high resolution TEM images and

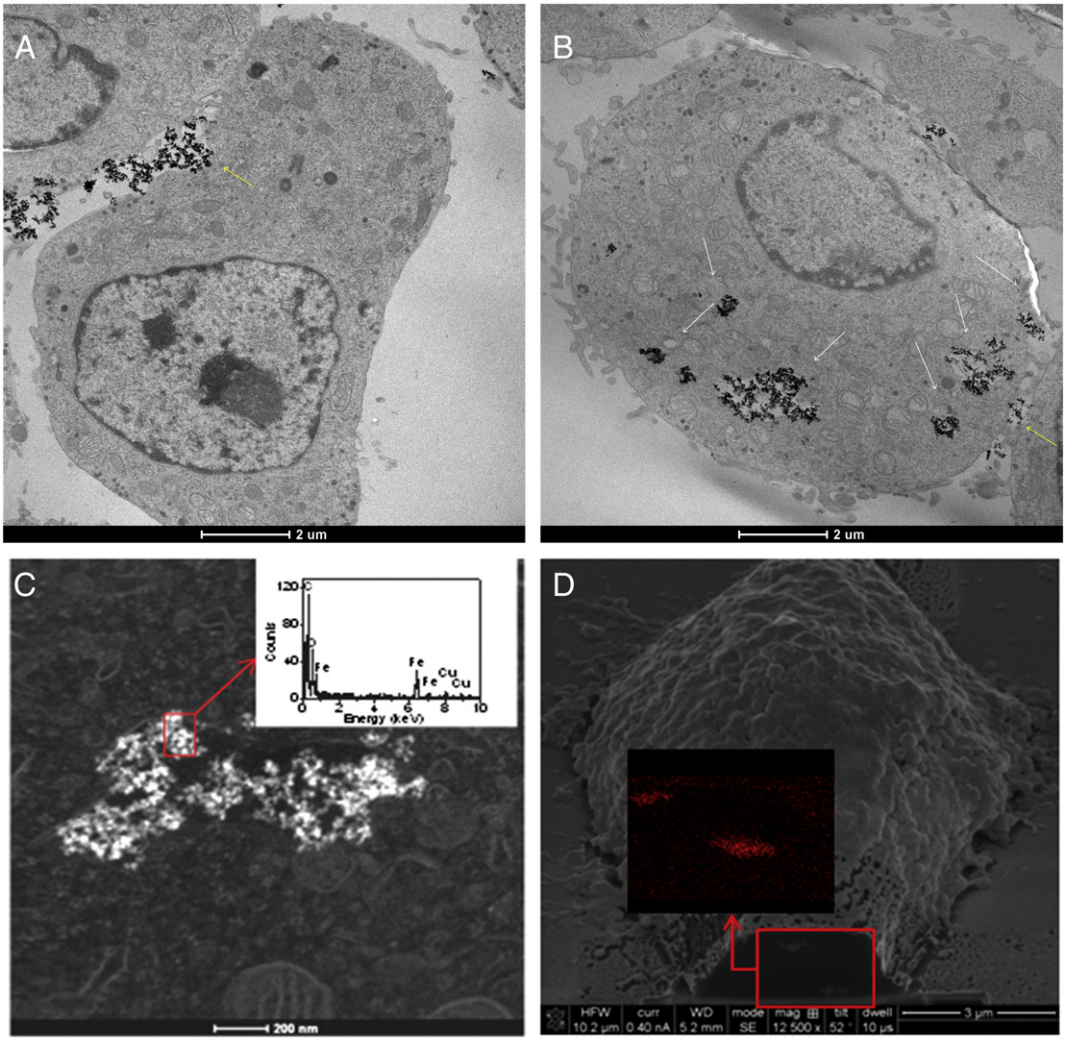

Figure 4. Cellular localization of f-MNPs. **(A-B)** TEM analysis of PC12 cells incubated 24 h with f-MNPs 10 μgml^{-1}. White arrows: particles in the cytoplasm, yellow arrows: particles entering and membrane invagination; **(C)** STEM-HAADF image (−173 °C) of PC12 cells incubated 24 h with f-MNPs 10 μgml^{-1}. Inset: EDS spectrum of cytoplasmatic f-MNPs; **(D)** SEM/FIB of PC12 cells incubated 72 h with f-MNPs 10 μgml^{-1}: cross section of a single cell; inset: EDS analysis of f-MNPs in the growth cone of the cell.

confirmed by Z-potential, infrared and XPS spectroscopy.[28] The total mass of PEI in the particles was around 14% (w/w) and the amount of the PEI on the particle surface was estimated 10 ± 2 μg per mg of MNPs (supplementary material). PEI offers primary and secondary amine-groups that have been used to functionalize the particles with a fluorescently labelled NGF-β (NGF_{fluor}). This fluorescent protein was achieved by covalent reaction between a protein mixture (NGF-β /BSA 1:6 w/w) and Alexa Fluor 488. The degree of the labelling was about 1.5 mol of dye per mole of protein (n = 6) and the efficiency of the labelling process was about 90% (n = 6) (supplementary material). The conjugation of the MNPs to the labelled protein (f-MNP) was achieved by electrostatic interactions. The shift towards negative values of Z-potential of f-MNPs compared to naked MNPs provides evidence of the absorption of the labelled protein on the surface of the MNPs (Figure 2). f-MNPs were tested on PC12 cells as these possess specific cell surface receptors that bind NGF.[30] In the presence of this growth factor, cells undergo a dramatic change in phenotype wherein they acquire a large part of the characteristic properties of sympathetic neurons. PC12 cells treated with the complex f-MNPs were found to exhibit a phenotype similar to the control culture (Figure S3, supplementary material). This result was confirmed by Western Blot analysis. It is known that NGF activates TrkA receptor leading to its phosphorylation (p-TrkA).[31] The antibody against p-TrkA (Tyr490), which detects endogenous levels of TrkA only when activated by NGF (i.e., phosphorylated at tyrosine 490), was used to analyse the levels of PC12 cell differentiation. The analysis confirmed that the fluorescent labelling of NGF-β did not alter the bio-functionality of the protein, which is also preserved after the conjugation with MNPs. Interestingly, experimental data demonstrated that the f-MNP complex is also stable when mixed to the cell culture medium, which indicates that non-specific adsorption of plasma proteins does not alter the stability and the integrity of the conjugate (Figure 3). Minimal cytotoxicity is another crucial requirement for any biomedical application. In a concentration range of 5-100 μgml^{-1}, a negligible cytotoxicity (<5%) was found after 72 h of incubation with the particles. Similarly, the

addition of the particles to the culture medium did not significantly interfere with the replication rate (Table 1). The trafficking of the particles inside the cells was monitored by TEM analysis (Figure 4, *A-B*). Particles appeared to enter the cells by an endocytic-like pathway. A cluster of particles was localised on the cell membrane which engulfs (Figure 4, *A-B*, yellow arrows) them forming vesicles which internalise the particles in the cytoplasm (Figure 4, *A-B*, white arrows). No particles were detected in nuclei and no damages at the cytoplasmatic organelles were found.

The presence of Fe inside the cells was confirmed by STEM-HAADF images and EDS spectra. In this mode, the sample is scanned with a small probe (around 1 nm in diameter) and an image and a spectrum can be collected simultaneously. Only electrons scattered at very high angles are collected in an annular detector to form the image, which is very sensitive to variations in atomic number. This technique is ideal for the identification of metallic particles in organic tissues. Thus, iron-based nanoparticles appear with a much brighter contrast in the image (Figure 4, *C*). The collection of EDS spectra proved the presence of iron material inside the cells (inset Figure 4, *C*). SEM analysis allowed to study the internal distribution of particles in adherent cells. EDS spectra performed on differentiated PC12 cells cross-sectioned by FIB/SEM confirmed the particle localization also in the growth cone of the cells (Figure 4, *D* and Figures S4-5 of supplementary material).

The aim of the present work was to demonstrate that MNPs can be exploited to manipulate axons/neurites under external magnetic forces for directing their orientation. Experiments were carried out in 3-cm Ibidi Petri dishes placed inside a Halbach-like cylinder magnetic applicator, which provided a constant magnetic field gradient of 46.5 Tm^{-1} in the radial direction. In this set-up, cells are exposed to the same magnetic force which is proportional to the magnetic field gradient, independent from the magnetic field value and with the radial outward direction (Figure 5). We measured the angles between the long axis of the neurites and the radial outward direction (i.e., direction of the magnetic force). The evidence that the synergic combination of f-MNPs and magnetic field influences the orientation of growing neuronal processes is shown in Figure 6. Specifically, in cells treated with f-MNPs, the exposure to the magnetic field induces neurites to grow preferentially along the direction of the magnetic force. Furthermore, experimental evidences demonstrated that neither the functionalised MNPs nor the magnetic field alone influences the direction of the neurite growth (Figure 6, *A*). The median value of the orientation index in the absence of particles and magnetic field was 0.006. This value was not statistically significant different from that obtained when the magnetic field was applied (0.001, $P = 0.61$) or cells are treated with f-MNPs (0.07; $P = 0.54$). As opposite, the neuronal processes tend to be arranged parallel to the magnetic force in the presence of both f-MNPs and magnetic field and the median value of the orientation index was 0.57 which was much higher than those in all other groups ($P < 0.001$). Cells treated with both particles and magnetic fields thus have a narrow angle distribution, i.e., cells are preferentially aligned to the radial direction compared to the other groups. Figure 6, *B* represents the trend of the angle distribution in presence of f-MNPs (f-MNP^+, M^-) or the magnetic field (f-MNP^-, M^+) or both (f-MNP^+, M^+), normalised with respect to the control (f-MNP^-, M^-). This representation clearly shows that cells treated f-MNPs alone or magnetic field alone have the same angle distribution of the control, in contrast with cells treated with both f-MNPs and magnetic field.

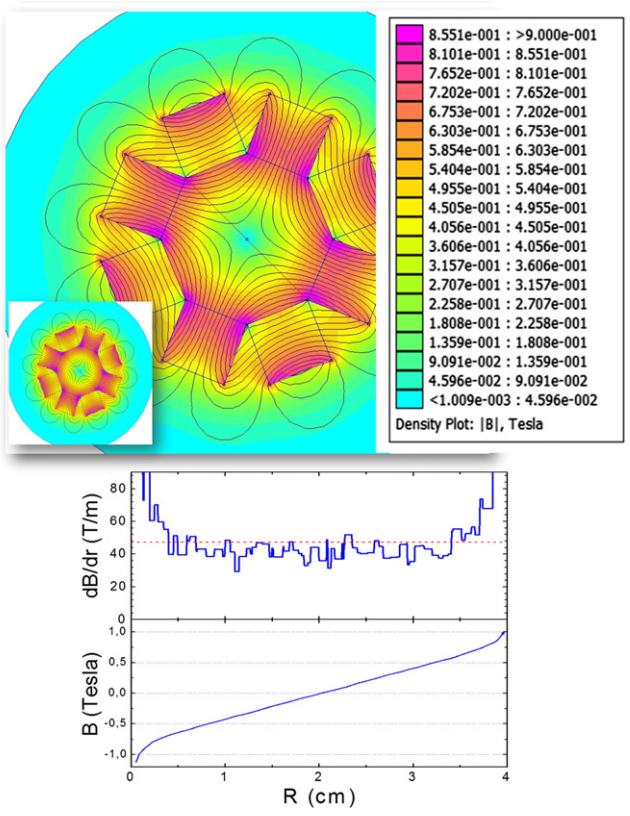

Figure 5. FEM modeling of the magnetic field inside the magnetic applicator. Top panel: Flux density *B* distribution inside the magnetic applicator, calculated from finite element simulation of the NdFeB magnet array. Bottom panel: graphs of tangential flux density *B(T)* and derivative $\frac{dB}{dr}$ (Tm^{-1}) along the radial direction inside the applicator. The dotted line is an average value for $\frac{dB}{dr}$ estimated in 46.5 Tm^{-1}.

Discussion

The iron oxide nanoparticles, synthesized by our team, offer a high saturation magnetization and a low cytotoxic profile.[28] They were functionalised with NGF-β for gaining specificity and triggering PC12 differentiation. In PC12 cells cultured with the f-MNPs, the particles were found to localize intracellularly by endocytosis and no signs of cytotoxicity could be detected. Similar results have been described in a number of studies reported in literature to evaluate the potential toxicity of superparamagnetic iron oxide nanoparticles (SPION).[32] Works in literature refer that SPIONs are quickly taken up by PC12 and the cellular uptake involves endocytosis.[33] SPIONs degrade in some intracellular endosomes/lysosomes between few days from administration. Specifically, SPION-containing endosomes were found to fuse with lysosomes, causing rapid dissociation at low

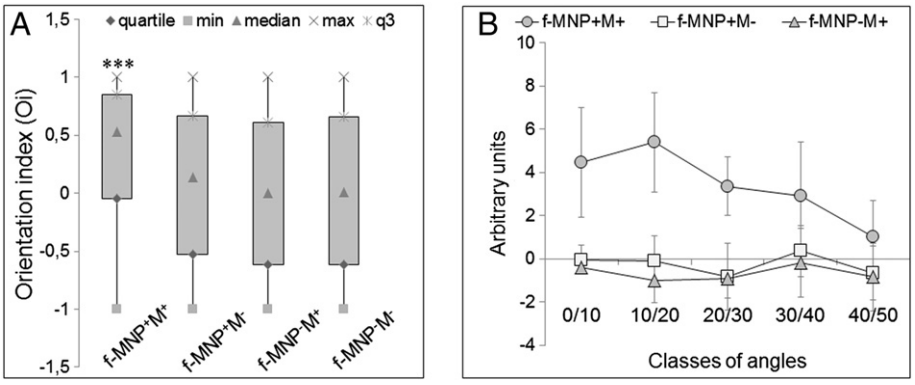

Figure 6. Effect of f-MNPs and magnetic field on the orientation of neuronal processes of PC12 cells. Four experimental groups were tested: cells treated with both f-MNPs and the magnetic field (f-MNP$^+$, M$^+$), with f-MNPs and a null magnetic field (f-MNP$^+$, M$^-$), without f-MNPs and the magnetic field (f-MNP$^-$, M$^+$) or without f-MNPs and a null magnetic field (f-MNP$^-$, M$^-$). **(A)** Neurite orientation index: the box-plot shows the median, interquartile ranges, the max and the minimum value. Dunnett's test ***$P < 0.001$ n = 6. **(B)** Number of neurites (normalised with respect to the control: f-MNP$^-$, M$^-$) grouped for classes of angles they form with the radial direction outwards.

pH of the iron core in soluble Fe(III), progressively incorporated into the iron-storing proteins.[34,35] Most importantly, our f-MNPs were found not only in endosomes/lysosomes but also in the cone growth of developing neurites.

In this work, we have demonstrated that f-MNPs and external magnetic fields can influence the growth direction of neurites, aligning them preferentially to the direction of the magnetic force. We assume that the mechanism involved in the re-direction of the neurites could be ascribed to the magnetic force acting on the MNP-bound neurite, which allows manipulation and orientation of the axons in order to orient and to overcome inhibitory factors.

A physical explanation of the obtained results is provided in the following. In a non-uniform magnetic field, the net force F exerted on a magnetic nanoparticle with magnetic moment m is given by:

$$F = (m \cdot \nabla) B \tag{1}$$

In our experimental set-up, the only non-null component of the magnetic field gradient is the radial one (dB/dr = 46.5 Tm^{-1}). As we found a value of saturation magnetization M_s of 58 Am^{2}kg^{-1} and a coercive field H_c of 4.81 kAm^{-1},[12] we can assume that particle magnetization saturated and Eq. (1) becomes:

$$F = m_s \frac{dB}{dr} = \rho V M_s \frac{dB}{dr} \sim 1.1 \cdot 10^{-16} N \tag{2}$$

Where ρ is the particle density and V the MNP volume.

Mass of f-MNPs up-taken by PC12 cells was calculated from the corresponding saturation magnetization M_s per cell at T = −23.17 °C as described in Fass and Odde[12] and it was found 9.9 ± 0.2 pg corresponding to a number of particles per cell $n_{cell}^{MNP} \sim 2.5 \cdot 10^5$. A single neurite will be thus subjected to a force F_{neur} given by the (2) multiplied for the number of magnetic particles entrapped in the neurite:

$$F_{neur} = n_{neur}^{MNP} F \tag{3}$$

We assume a uniform particle distribution in cell cytoplasm:

$$n_{neur}^{MNP} = n_{cell}^{MNP} \frac{V_{neur}}{V_{cytop}} \tag{4}$$

Where V_{cytop} and V_{neur} are the cell cytoplasm volume and neurite volume, respectively. In a polar coordinate system, where the origin is the neurite origin, the radial component $\hat{r}$ is the neurite direction and the angular component is $\hat{\theta}$, this force has two components, the radial $F^r_{neur} = F_{neur} \cos\theta$ and the angular $F^\theta_{neur} = F_{neur} \sin\theta$. The latter is the effective component for orienting the neurite (the first stretch the neurite along its axis).

We modeled the neurite as a rigid semi-cone with height l and radius r, anchored to the substrate with bridges (n_b is the number of bridges per unit of surface and ε is their spring constant). Adhesion is promoted by the positive charges on poly-L-lysine which attract the negative charges of cell membrane due to the

Table 2
Parameters used in mathematical model.

Parameter	Descriptions	Value	Ref
ρ	Particle density	5000 kgm^{-3}	*
V	MNP volume	$8.2 \cdot 10^{-24}$ m^3	*
V_{cytop}	Cell cytoplasm volume	$4.41 \cdot 10^{-16}$ m^3	*
S	Cell adhesion surface	$7.2 \cdot 10^{-11}$ m^3	*
r	Neurite radius	$7.5 \cdot 10^{-7}$ m	*
n_{cell}^{MNP}	Number of MNPs per cell	$2.5 \cdot 10^5$	*
$l(t_f)$	Neurite length at t_f	$3.6 \cdot 10^{-6}$ m	*
ε	Spring constant value	$2.4 \cdot 10^{-4}$ N/m	49
N_b	Number of bridge for cell	$\sim 5 \cdot 10^4$	50

Those marked with * are experimentally evaluated.

Table 3
Analysis of neurite length (n=6, p=0.08) and neurite number per cell (n=6, p=0.42).

	f-MNP$^+$, M$^+$	f-MNP$^+$, M$^-$	f-MNP$^-$, M$^+$	f-MNP$^-$, M$^-$
Neurite length (μm)	36.5 [21.7-54.5]	25.5 [17.6-44.2]	30.2 [23.7-40.0]	26.1 [18.7-38.2]
Neurite number per cell	2 [2-3]	2 [1-3]	2 [2-3]	2 [1-3]

One-way ANOVA.

glycocalyx. This induces an electrostatic bond formation, similar to the ligand-receptor-mediated interaction.[36]

To model mathematically the phenomenon, we will use a simple model, already validated in our previous studies.[37] Applying the Bell theory to a receptor-ligand bond, the bond lifetime τ when the cell is stressed by the external force is given by[38,39]:

$$\tau = \tau_0 e^{\left(\frac{E_0 - r_s f}{kT}\right)} \quad (5)$$

where E_0 is the free energy change on binding, r_s is the binding cleft, f is the force applied per bond and $kT = 4.1 \cdot 10^{-21}$ J is the thermal energy. In the literature, for a representative antigen–antibody bond, E_0 is estimated about $5.9 \cdot 10^{-20}$ J, the binding cleft $r_s = 0.5$ nm, within a factor of 2, and τ_0 in the order of 10^{-8} s.[40]

Bonds in cell adhesion will therefore be continually created, loaded over some period of time, then fail. Under the effect of the angular component of the force acting on the bond, dynamic process of bond loading, failure, and formation drives cytoskeletal movements, resulting in a displacement of l(t) Δθ at any time τ.

By imposing the equilibrium on the neurite:

$$F^{\theta}_{neur}(\theta, t) = 2\varepsilon \triangle\theta \frac{r}{l(t)} \sum_{1}^{\frac{l(t)}{a}} i(l(t) - ia) = \frac{1}{3}\varepsilon \triangle\theta r \left[\left(\frac{l(t)}{a}\right)^2 - 1\right] \quad (6)$$

where

$$a = {}^{1}/_{\sqrt{n_b}}.$$

We imposed the following boundary conditions: $t_0 = 0$ (time of application of the magnetic field), $\theta(t_0) = \frac{\pi}{2}$ (Figure 6, median value of f-MNP$^-$M$^-$) and the length l increases linearly over the time from $t_s = -24$ h (application of the differentiating stimulus) to $t_f = 72$ h (time lapse of the experiment).

By substituting in Eq. 6 the values reported in Table 2 and solving the equation, we found $\theta(t_f) \sim \frac{\pi}{3}$ which is in optimal agreement with our experimental data (Figure 6, median value of f-MNP$^+$M$^+$).

This corresponds to a net neurite angle displacement of $\sim \frac{\pi}{6}$ in the time of the experiment. Additionally the proposed model allows to theorize which are the key parameters controlling the process, i.e., the magnetization of the particles, the strength of the applied magnetic field and the amount of particles interacting with the neuronal process. These parameters should be carefully optimized time by time, depending on the experimental set-up, and this is particularly relevant for planning future in vivo experiments.

This finding represents the first demonstration that the synergic use of MNPs and M can influence the orientation of the neuronal growth processes. M alone has no influence on the direction of newly formed neurites of PC12 cells, although a previous work by Kim et al[41] reported that neurites grew preferentially in a direction perpendicular to the direction of a static magnetic field. These results are difficult to interpret because details of the magnetic field and magnetic gradient used were not provided, and thus the direction of the generated magnetic force cannot be correlated with preferential direction of growth. The same authors reported that 11 nm iron oxide nanoparticles (in absence of magnetic field) enhance in a dose-dependent manner the neurite outgrowth of PC12 cells exposed to both particles and NGF. The authors suggested a mechanism in which iron triggers the activation of cell adhesion molecules that are associated with cell matrix interactions.[42]

Concerning the length distribution of neurites, we observed a trend toward statistical significance ($P = 0.08$, one-way ANOVA) with the higher values for cells treated with both the particles and the magnetic field (38% over the control f-MNP$^-$M$^-$, corresponding to an increase in the elongation rate of about 0.14 μmh^{-1}) (Table 3), according to the role of forces in neurite lengthening.[13]

We have no evidence of enhanced neurite initiation as neurite number seems not to be influenced in any experimental group tested ($P = 0.42$, one-way ANOVA) (Table 3), coherently with data reported in literature which refer that forces typically required for experimentally induced neurite initiation from PC12 cells are in the range of 3-10 nN.[43]

Of note, our protocol allows the application of force in the pN range (30 pN at whole cell level, below 1 pN at neurite level) over long times (days). In previous works, force was applied to neurons for determination of the relationship between applied tensions and elongation rate with calibrated glass needles as described by Lamoureux et al and Zheng et al[43,44]: a calibrated needle is generally used to apply a constant force and the neurite is pulled in steps of 30-60 min; tension is usually varied between 0.1 and 10 nN. By using this methodology, the rate of neurite elongation in PC12 cells and chick sensory neurons was found to be a function of the applied force above some minimum threshold tension (usually around 1 nN)[44,45] and the elongation rate was found similar for both peripheral and central neurons (about 1 μmh^{-1} per 10 pN of applied force)[44.46] However, the effects of very low tensions over longer time scale (days) have been very poorly investigated because glass microneedle technique does not allow to apply and study the effect of pN forces on cells and their processes. This is exemplified by two studies on forebrain neurons. By using glass microneedle technique Chada et al did not detect a minimum threshold tension required for elongation[46] while it was observed by Fass et al who used magnetic beads to apply force with greater accuracy and precision in the pN range.[12] Additionally, microneedle

methodology applies a minimum force of 0.1 nN which is too crude to investigate effects on neurons over a time scale longer than 1 h.

Here we report the use of a MNP-based technique for application of very low mechanical tensions (range of pN) which could be used to systematically investigate the role of force on neurite direction and elongation at longer time scales. An important aspect of our work and similar studies reported in literature[47,48] is thus that forces need to be applied at low levels over long time periods (generally days, 72 h in our study).

In conclusion, our results showed that the multifunctional nanoparticles could be efficient agents for magnetically-driven "actuation" of growing neuronal processes. In addition to the evidence that mechanical tension created by MNPs can induce "stretch growth" of neurites or process initiation,[12] we demonstrated that it is also able to support "physical guidance" for directing the outgrowth process and this mechanism occurs by applying very low forces (in the pN range). Together with the previously published results, our findings indicate that forces, when carefully controlled, could act as powerful stimulants of neurite development. The tension produced by MNPs could contribute to the successful treatment of lesions to the peripheral nervous system or central nervous system which have, until very recently, been considered incurable. Obviously, further work is required to translate these findings on models of nerve regeneration and validate them in-vivo.

Appendix A. Supplementary data

Supplementary data to this article can be found online at http://dx.doi.org/10.1016/j.nano.2013.12.008.

References

1. Isaacs J. Treatment of acute peripheral nerve injuries: current concepts. *J Hand Surg-Am* 2010;**35A**:491-7.
2. Schmidt CE, Leach JB. Neural tissue engineering: strategies for repair and regeneration. *Annu Rev Biomed Eng* 2003;**5**:293-347.
3. Gordon T. The physiology of neural injury and regeneration: the role of neurotrophic factors. *J Commun Disord* 2010;**43**:265-73.
4. Dickson BJ. Molecular mechanisms of axon guidance. *Science* 2002; **298**:1959-64.
5. Daly W, Yao L, Zeugolis D, Windebank A, Pandit A. A biomaterials approach to peripheral nerve regeneration: bridging the peripheral nerve gap and enhancing functional recovery. *J R Soc Interface* 2012;**9**: 202-21.
6. Murugan R, Ramakrishna S. Design strategies of tissue engineering scaffolds with controlled fiber orientation. *Tissue Eng* 2007;**13**:1845-66.
7. Gulati AK, Cole GP. Immunogenicity and regenerative potential of acellular nerve allografts to repair peripheral-nerve in rats and rabbits. *Acta Neurochir* 1994;**126**:158-64.
8. Dubey N, Letourneau PC, Tranquillo RT. Guided neurite elongation and Schwann cell invasion into magnetically aligned collagen in simulated peripheral nerve regeneration. *Exp Neurol* 1999;**158**:338-50.
9. Franze K, Guck J. The biophysics of neuronal growth. *Rep Prog Phys* 2010;**73**:094601 (19pp).
10. Bray D. Mechanical tension produced by nerve-cells in tissue-culture. *J Cell Sci* 1979;**37**:391-410.
11. Bray D. Axonal growth in response to experimentally applied mechanical tension. *Dev Biol* 1984;**102**:379-89.
12. Fass JN, Odde DJ. Tensile force-dependent neurite elicitation via anti-beta 1 integrin antibody-coated magnetic beads. *Biophys J* 2003;**85**:623-36.
13. Suter DM, Miller KE. The emerging role of forces in axonal elongation. *Prog Neurobiol* 2011;**94**:91-101.
14. Lowery LA, Van Vactor D. The trip of the tip: understanding the growth cone machinery. *Nat Rev Mol Cell Biol* 2009;**10**:332-43.
15. Spivey EC, Khaing ZZ, Shear JB, Schmidt CE. The fundamental role of subcellular topography in peripheral nerve repair therapies. *Biomaterials* 2012;**33**:4264-76.
16. Fan YW, Cui FZ, Hou SP, Xu QY, Chen LN, Lee IS. Culture of neural cells on silicon wafers with nano-scale surface topograph. *J Neurosci Meth* 2002;**120**:17-23.
17. Yang F, Murugan R, Ramakrishna S, Wang X, Ma YX, Wang S. Fabrication of nano-structured porous PLLA scaffold intended for nerve tissue engineering. *Biomaterials* 2004;**25**:1891-900.
18. Mitchel JA, Hoffman-Kim D. Cellular scale anisotropic topography guides Schwann cell motility. *Plos One* 2011;**6**:e24316.
19. Schenck JF. Safety of strong, static magnetic fields. *J Magn Reson Imaging* 2000;**12**:2-19.
20. Pankhurst QA, Connolly J, Jones SK, Dobson J. Applications of magnetic nanoparticles in biomedicine. *J Phys D-Appl Phys* 2003;**36**: R167-81.
21. Jain TK, Richey J, Strand M, Leslie-Pelecky DL, Flask CA, Labhasetwar V. Magnetic nanoparticles with dual functional properties: drug delivery and magnetic resonance imaging. *Biomaterials* 2008;**29**:4012-21.
22. Maier-Hauff K, Ulrich F, Nestler D, Niehoff H, Wust P, Thiesen B, et al. Efficacy and safety of intratumoral thermotherapy using magnetic iron-oxide nanoparticles combined with external beam radiotherapy on patients with recurrent glioblastoma multiforme. *J Neuro-Oncol* 2011; **103**:317-24.
23. Riggio C, Calatayud MP, Hoskins C, Pinkernelle J, Sanz B, Torres TE, et al. Poly-L-lysine-coated magnetic nanoparticles as intracellular actuators for neural guidance. *Int J Nanomedicine* 2012;**7**:3155-66.
24. Goncalves NP, Oliveira H, Pego AP, Saraiva MJ. A novel nanoparticle delivery system for in vivo targeting of the sciatic nerve: impact on regeneration. *Nanomedicine* 2012;**7**:1167-80.
25. Pilakka-Kanthikeel S, Atluri VSR, Sagar V, Saxena SK, Nair M. Targeted brain derived neurotropic factors (BDNF) delivery across the blood–brain barrier for neuro-protection using magnetic nano carriers: an in-vitro study. *Plos One* 2013;**8**:e62241.
26. Steketee MB, Moysidis SN, Jin XL, Weinstein JE, Pita-Thomas W, Raju HB, et al. Nanoparticle-mediated signaling endosome localization regulates growth cone motility and neurite growth. *Proc Natl Acad Sci U S A* 2011;**108**:19042-7.
27. Sugimoto T, Matijevic E. Formation of uniform spherical magnetite particles by crystallization from ferrous hydroxide gels. *J Colloid Interf Sci* 1980;**74**:227-43.
28. Calatayud MP, Riggio C, Raffa V, Sanz B, Torres TE, Ricardo Ibarra M, et al. Neuronal cells loaded with PEI-coated Fe3O4 nanoparticles for magnetically-guided nerve regeneration. *J Mater Chem* 2013;**1**:3607-16.
29. Akritas MG. The rank transform method in some 2-factor designs. *J Am Stat Assoc* 1990;**85**:73-8.
30. Landreth GE, Shooter EM. Nerve growth-factor receptors on Pc12 cells — ligand-induced conversion from low-affinity to high-affinity states. *P Natl Acad Sci-Biol* 1980;**77**:4751-5.
31. Kaplan DR, Hempstead BL, Martin-Zanca D, Chao MV, Parada LF. The trk proto-oncogene product: a signal transducing receptor for nerve growth factor. *Science* 1991;**252**:554-8.
32. Ito A, Shinkai M, Honda H, Kobayashi T. Medical application of functionalized magnetic nanoparticles. *J Biosci Bioeng* 2005;**100**:1-11.
33. Pisanic TR, Blackwell JD, Shubayev VI, Finones RR, Jin S. Nanotoxicity of iron oxide nanoparticle internalization in growing neurons. *Biomaterials* 2007;**28**:2572-81.
34. Arbab AS, Wilson LB, Ashari P, Jordan EK, Lewis BK, Frank JA. A model of lysosomal metabolism of dextran coated superparamagnetic

iron oxide (SPIO) nanoparticles: implications for cellular magnetic resonance imaging. *Nmr Biomed* 2005;**18**:383-9.
35. Lunov O, Syrovets T, Rocker C, Tron K, Nienhaus GU, Rasche V, et al. Lysosomal degradation of the carboxydextran shell of coated superparamagnetic iron oxide nanoparticles and the fate of professional phagocytes. *Biomaterials* 2010;**31**:9015-22.
36. Rainaldi G, Calcabrini A, Santini MT. Positively charged polymer polylysine-induced cell adhesion molecule redistribution in K562 cells. *J Mater Sci-Mater M* 1998;**9**:755-60.
37. Raffa V, Vittorio O, Ciofani G, Pensabene V, Cuschieri A. Cell creeping and controlled migration by magnetic carbon nanotubes. *Nanoscale Res Lett* 2010;**5**:257-62.
38. Evans EA, Calderwood DA. Forces and bond dynamics in cell adhesion. *Science* 2007;**316**:1148-53.
39. Bell GI. Theoretical-models for the specific adhesion of cells to cells or to surfaces. *Adv Appl Probab* 1980;**12**:566-7.
40. Hynes RO. Cell adhesion: old and new questions. *Trends Biochem Sci* 1999;**24**:M33-7.
41. Kim S, Im WS, Kang L, Lee ST, Chu K, Kim BI. The application of magnets directs the orientation of neurite outgrowth in cultured human neuronal cells. *J Neurosci Meth* 2008;**174**:91-6.
42. Kim JA, Lee NH, Kim BH, Rhee WJ, Yoon S, Hyeon T, et al. Enhancement of neurite outgrowth in PC12 cells by iron oxide nanoparticles. *Biomaterials* 2011;**32**:2871-7.
43. Lamoureux P, AltunGultekin ZF, Lin CJ, Wagner JA, Heidemann SR. Rac is required for growth cone function but not neurite assembly. *J Cell Sci* 1997;**110**:635-41.
44. Zheng J, Lamoureux P, Santiago V, Dennerll T, Buxbaum RE, Heidemann SR. Tensile regulation of axonal elongation and initiation. *J Neurosci* 1991;**11**:1117-25.
45. Dennerll TJ, Lamoureux P, Buxbaum RE, Heidemann SR. The cytomechanics of axonal elongation and retraction. *J Cell Biol* 1989;**109**:3073-83.
46. Chada S, Lamoureux P, Buxbaum RE, Heidemann SR. Cytomechanics of neurite outgrowth from chick brain neurons. *J Cell Sci* 1997;**110**:1179-86.
47. Pfister BJ, Bonislawski DP, Smith DH, Cohen AS. Stretch-grown axons retain the ability to transmit active electrical signals. *FEBS Lett* 2006;**580**:3525-31.
48. Yi CJ, Dahlin LB. Impaired nerve regeneration and Schwann cell activation after repair with tension. *Neuroreport* 2010;**21**:958-62.
49. Dennerll TJ, Joshi HC, Steel VL, Buxbaum RE, Heidemann SR. Tension and compression in the cytoskeleton of Pc-12 neurites. II — quantitative measurements. *J Cell Biol* 1988;**107**:665-74.
50. Sabri S, Soler M, Foa C, Pierres A, Benoliel AM, Bongrand P. Glycocalyx modulation is a physiological means of regulating cell adhesion. *J Cell Sci* 2000;**113**:1589-600.